JOURNAL OF MATERIALS SCIENCE 33 (1998) 287–303

Orientation-dependent mechanical properties and deformation morphologies for uniaxially melt-extruded high-density polyethylene films having an initial stacked lamellar texture

HONGYI ZHOU, G. L. WILKES*
Chemical Engineering Department, Polymer Materials Interfaces Laboratory, Virginia Polytechnic Institute and State University, Blacksburg, VA 24061, USA

The mechanical properties and the associated plastically deformed morphologies of high density polyethylene films were investigated by tensile testing, wide-angle X-ray scattering and transmission electron microscopy. Uniaxially oriented films having a well-defined stacked lamellar morphology, both with and without row-nucleated structure were deformed at three angles, 0°, 45° and 90°, with respect to the original machine (extrusion) direction. A distinct orientation dependence of the mechanical properties was observed and this dependence has been related to the different morphologies developed during the plastic deformation processes. It was shown that lamellar separation, lamellar shear and lamellar break-up were the dominant initial deformation mechanisms for the respective 0°, 45° and 90° deformations. As a result, the 45° and 90° deformations generated a final microfibril morphology oriented along the stretch direction, while the 0° deformation resulted in broken blocks of crystalline lamellae. The presence of distinct row-nucleated crystalline fibrils in the initial structure stiffens the material in the 0° deformation; however, it significantly limits the ability of the materials to cold draw at the 90° deformation. Morphological models were proposed to explain the plastic deformation process for the different deformation angles, as well as for the deformation behaviour of semicrystalline polymers with an isotropic spherulitic morphology.

1. Introduction

Polymers represent a very important and still rapidly growing class of engineering materials. Among them, semicrystalline polymers are of particular interest. Often, their remarkable drawability makes it possible to highly orient them in the solid state. Solid-state processing techniques, such as drawing fibres or stretching films, depend upon the plastic deformation characteristics of the given polymer. During solid-state processing, macromolecular chains are often preferentially oriented along a specific direction, e.g., the machine direction, so that the final products possess the desired properties at a particular orientation, this generally being the loading direction in most applications. From an engineering point of view, in order to manipulate the final properties of the materials, it is important to understand the physical orientation process and therefore to be able to control the orientation state of both the crystalline and the amorphous phases. On the other hand, the detailed molecular rearrangement in the process of plastic deformation is also an interesting topic for fundamental research. Thus, it is not surprising that there has been a tremendous amount of research that has been focused on this area [1–10].

Semicrystalline polymers that crystallize under quiescent conditions often have a spherulitic morphology. For these unoriented semicrystalline polymers, there are three basic levels of microstructures that are important in the deformation process [11]: (i) the 2–20 Å level, which represents the interactions between neighbouring chain segments in both the crystalline phase and the amorphous phase; (ii) the 100–300 Å level, which represents the thickness of the crystalline lamellae and of the amorphous layers between the crystalline lamellae; (iii) the 0.5–100 μm level, which represents the dimension of larger-scale superstructures such as spherulites, which are complex arrangements of crystalline lamellae and amorphous regions. Therefore, semicrystalline polymers possessing a spherulitic morphology must be regarded as microstructural and mechanical complex systems, as depicted in Fig. 1 (according to [12]), in which all the three subregions of a spherulite influence the

*To whom all correspondence should be directed.

0022–2461

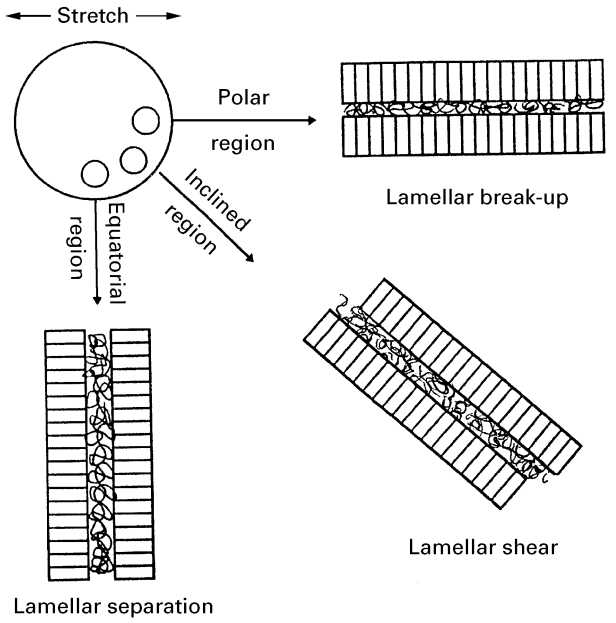

Figure 1 A schematic drawing that shows the complexity in the deformation of spherulitic morphology.

deformation process. Certainly, there are cases where all the above three levels are not always present such as semicrystalline polymers that have already undergone extensive drawing.

A variety of experimental techniques have been utilized to investigate the morphological changes during the plastic deformation process at the three structural levels: optical microscopy [13], scanning electron microscopy (SEM) [14–17], transmission electron microscopy (TEM) [18–27], atomic force microscopy (AFM) [28–30], electron diffraction [31, 32], small-angle light scattering (SALS) [33], wide-angle X-ray scattering (WAXS) and small-angle X-ray scattering (SAXS) [34–50], small-angle neutron scattering (SANS) [51–54], infrared spectroscopy [41, 55], Raman spectroscopy [41, 45, 56], electron paramagnetic resonance [57], differential scanning calorimetry (DSC) [58], dynamic mechanical thermal analysis [59], stress–strain deformation [60] and microhardness [61]. Most of the studies quoted above have utilized high-density polyethylene (HDPE) as a model material because of not only its high commercial importance but also its *relatively* simple backbone chemical structure and better understood crystallization behaviour and morphology as well.

In the following paragraphs, and utilizing HDPE as the principal example, a brief overview is provided to summarize the current understanding about the deformation mechanisms and the final morphologies for semicrystalline polymers, obtained primarily by X-ray scattering and electron microscopy studies. More thorough and detailed reviews can be obtained from [1–10], especially [2, 3, 8]. By combining the use of SAXS and WAXS, *either real-time or via post-deformation investigations*, it has been possible to detect the deformation processes at the crystalline lamellae and amorphous interlayer level as well as at the crystallographic level. With the help of electron microscopy, particularly TEM, more details of the locally deformed morphologies of crystalline lamellae have been observed and have generally confirmed the deformation mechanisms proposed on the basis of X-ray scattering experiments.

According to the theory of crystal plasticity, which was originally developed for metals, plastic deformation at the crystallographic level can be achieved by three different mechanisms, namely, slip, mechanical twinning and martensitic phase transformation [34–36]. Furthermore, the plastic deformation of semicrystalline polymers has also been considered as a decrystallization process, defined as mechanically induced destruction of crystalline lamellae (unfolding) followed by a recrystallization process [17, 51]. These two interpretations have been supported by some experimental results, but neither has successfully explained all the experimental observations. It appears that, at least for HDPE, yielding at or near room temperature is basically controlled by crystal plasticity processes while, for large post-yielding deformations, decrystallization and recrystallization are involved. However, by examining the final morphology of the deformed material, it seems impossible to distinguish the mechanisms by which the deformation may have occurred. Therefore, other techniques such as mechanical testing have to be used in conjunction with scattering and microscopy to understand this topic better.

(i) *Slip.* When the resolved shear stress on a particular slip plane in specific slip directions for a given crystal is larger than that of the critical shear stress for the slip system, dislocation motion occurs. The speculations about the existence of dislocations in polymer crystals has been confirmed by the formation of moiré fringes between crystalline lamellae by direct observation as well as by electron microscopy [32]. The long-chain nature of polymer crystals requires that the *most preferred* slip plane contains the polymer chains, meaning that the slip planes must be of the $\{h\,k\,0\}$ types (assuming that the c axis is parallel to the chain axis and chain folding is of tight folds) such that the polymer chains remain unbroken during slip. Slip can be either in the chain direction (*chain slip*), which is the dominant event, or perpendicular to the chain direction (*transverse slip*), which is further restricted to the chain-folding planes to prevent the disruption of the chain folds of the crystalline lamellae. It is expected that chain slip must be influenced by the nature of chain folding, such as fold tightness and chain re-entry. It is also expected that crystallization kinetics can affect the feasibility of chain slip, i.e., it is certainly easier for chain slip to take place if the crystallization is confined within regime I, compared with the cases of regimes II and III, assuming the crystallization can be described by the regime theory [62].

From the WAXS and SAXS studies on stretched HDPE [35, 39], chain slip has been proposed to occur by two different routes for a slip system to achieve the same amount of strain. Deformation can be introduced by *fine slip*, where a small amount of slip occurs equally on a large number of parallel planes. On the contrary, the deformation can also be generated by

coarse slip (*block slip*), where slip takes place on fewer number of planes with a large amount of slip. Microscopically, fine slip results in a change in the angle between the molecular chain axis and the normal of the crystalline lamella, whereas for coarse slip this angle remains unchanged.

(ii) *Mechanical twinning and martensitic phase transformation.* According to the theory of crystal plasticity, other deformation modes, namely, mechanical twinning and martensitic phase transformation, can also produce plastic strain. Mechanical twinning is characterized by shearing part of a crystal with respect to a shear plane which is common for both the product and the parent crystals. The result of this is the formation of mirror symmetry with respect to the shear plane. Martensitic phase transformation is a strain-induced phase transition, where the product phase and the parent phase share a common invariant plane and/or a common invariant direction. Mechanical twinning has been detected on rolled HDPE by WAXS [34, 36], and the development of a monoclinic crystalline phase as a result of a martensitic phase transformation has also been found in the same study [36] as well as in other investigations for the cold-drawn polyethylene [41, 44–47, 49].

Again, the long-chain nature of polymers limits the shear and invariant planes for the mechanical twinning and martensitic phase transformation to the $\{h\,k\,0\}$ types. For HDPE, the proposed shear planes include $\{3\,1\,0\}$ and $\{1\,1\,0\}$, which result in lattice rotations about the chain axis by 55° and -67°, respectively. For martensitic phase transformation, the orthorhombic crystalline structure ($a = 0.742$ nm, $b = 0.495$ nm and $c = 0.254$ nm) is transformed into the monoclinic crystalline structure ($a = 0.809$ nm, $b = 0.479$ nm and $c = 0.254$ nm; $\gamma = 107.9^\circ$) at a shear strain of either 0.201 or 0.318, corresponding to two types of shear that can most favourably result in the transformation from the orthorhombic unit cell to that of the monoclinic unit cell [63]. It is necessary to point out, however, that the amount of strain produced by the latter two deformation modes are less than that from chain slip.

(iii) *Decrystallization and recrystallization processes.* According to this proposal, the dominant mechanism for yielding and further plastic deformation for semicrystalline polymers are sequential events of partial or local melting, stretching of the melted polymer chains, and recrystallization under the applied stress. When a polymer yields, the local temperature may rise through viscous heating in that region that undergoes necking, and this may cause the melting of crystalline lamellae in the necked region. The chains in the melt are then stretched towards the direction of the applied stress and finally recrystallize into an oriented microfibrillar crystalline phase. This process continues as necking proceeds along the specimen. By this route the original (spherulitic) structure is converted into a highly oriented microfibril structure which contains alternating crystalline lamellae and amorphous regions.

At the crystalline lamella and amorphous layer level, semicrystalline polymers can be regarded as consisting of crystalline lamellae separated by an amorphous phase and held together by tie chains, although the nature of the chain-folding surface and the adjacent amorphous phase as well as the exact physical state of the tie chains are still not completely understood owing to their complex dependence on chain chemistry, crystallization kinetics, processing, etc. In the light of the above consideration, three deformation modes, namely lamellar shear, lamellar separation and lamellar rotation, have been postulated as being associated with the deformation at this structural level.

(a) *Lamellar shear.* This deformation mode involves a simple shear of the amorphous regions between the crystalline lamellae, with the shear direction being parallel to the lateral direction of the crystalline lamellae. This deformation mode has been observed by SAXS for rolled HDPE [38]. It is believed that this deformation mode is relatively easy to induce since the amorphous phase is in a rubbery state at ambient temperature for HDPE. Also, it is interesting that WAXS and SAXS results suggest that, during the deformation process, lamellar shear and chain slip, which are relatively easy to promote, are in competition, i.e., lamellar shear-induced rotation of crystalline lamellae towards the applied stress direction and chain-slip induced rotation of chains towards the same stress direction provide constraints on each other [37].

(b) *Lamellar separation.* In the same experiments in which lamellar shear has been proposed [37, 38], the total change in the long spacing calculated from the SAXS data did not match that due to chain slip (corrected by chain tilting); therefore, lamellar separation was proposed and has successfully explained the experimental results. This deformation mode has been shown to be especially valid in the deformation of hard-elastic fibres owing to the special stacked lamellar morphology possessed by these fibres [25]. For HDPE, this deformation mode was found to be highly reversible, and this was believed to be due to the rubbery state of the amorphous phase [37]. In the case of hard-elastic fibres, the processes of elastic bending of the crystalline lamellae as well as an opening or splaying of the amorphous phase between the crystalline lamellae (resulting in a localized decrease in density) have been proposed [25].

(c) *Lamellar rotation.* The existence of this kind of deformation mode has initially been speculated to explain the fact that semicrystalline polymers can be deformed relatively easily, regardless of the fact that they rarely possess five independent slip systems which are necessary for a crystal to be deformed on the basis of crystal plasticity theory [64]. Later, such deformation was indeed observed by SAXS [37] and SEM [14] on stretched HDPE. In order to accommodate any structural distortion, it is often necessary for the crystalline lamellae to rotate in the process of deformation [6]. For HDPE, the rubbery amorphous phase makes it much easier for this to occur at room temperature. Therefore, although lamellar rotation does not produce any major strain by itself, it serves as an important process in which the crystalline lamellae can adjust themselves during the deformation process

to generate a larger amount of strain in the amorphous phase.

Based on both X-ray scattering and electron microscopy studies, several morphological models have been proposed to describe the plastic deformation process for semicrystalline polymers, more specifically the drawing process that transforms an isotropic spherulitic structure into a microfibril structure [65–70]. All the models share some of the basic deformation stages, while the differences lie in the elements of the final morphology as well as their origins. The basic deformation processes have been proposed as follows: the stressed spherulitic lamellae shear into crystal blocks by chain slip; then the crystal blocks rotate such that the polymer chains align towards the local principal stress directions. During this transition, the crystal blocks decrease in width, by chain slip and/or lamellar break-up (unfolding of crystalline lamellae), until a microfibrillar structure is formed, which is the basic structural element of these models.

In Peterlin's [65] model, the microfibrils are considered as being composed of alternating crystal blocks and amorphous regions connected by taut tie chains. Therefore, the modulus of a drawn semicrystalline polymers along the drawing direction is proportional to the number of the taut tie chains which serve as load transfer agents. Similar models have also been proposed by Prevorsek *et al.* [66] and Fischer and Goddar [67], in which the amount of the taut tie chains was related to the draw ratio of the respective drawn material. However, Porter [68] and Clark and Scott [69] suggested a different kind of extended-chain model, in which the microfibrils are considered as an extended-chain crystalline phase with chain ends being incorporated into the crystalline phase as defects. This type of model has been used to explain the ultrahigh modulus of the ultradrawn fibres. Furthermore, Clements *et al.* [70] proposed a third kind of model, which somewhat combines both features of microfibril models and the extended-chain model, i.e., the morphology of highly drawn semicrystalline polymers consists of stacks of crystalline lamellae linked by short crystalline bridges, in which polymer chains are in an extended-chain conformation. This model has also been used to explain the enhanced modulus of highly drawn fibres.

Given the above-mentioned massive, fruitful and sometimes imaginative investigations, there is still a need to display or observe clearly the development of the morphological changes during the deformation process for general semicrystalline polymers and, more importantly, to relate the observed morphology to the relevant mechanical properties of the materials. In most deformation studies on semicrystalline polymers, the WAXS and SAXS results have not been directly related to mechanical properties, i.e., the samples used for the mechanical tests and those for WAXS and SAXS experiments were either different or the same but without knowing the precise amount of strain. Although there were studies in which such an effort has been made [43, 47], they lacked direct support from either electron microscopy studies or mechanical testing. For the TEM studies, the majority of the investigations have utilized specially prepared ultrathin ultradrawn films that are suitable for direct TEM observation [32]. Although such films are excellent for direct visualization, they have often possessed a shish-kebab morphology, and the presence of the shishes certainly influences the deformation morphology and mechanical property of the films (see later discussion in this paper as well). Therefore, the conclusions drawn from the studies that have made use of the ultrathin ultradrawn films need to be further confirmed by comparable investigations by utilizing other more conventional morphological systems. Additionally, it is also hard to conduct mechanical tests on ultrathin films, although such a measurement has been reported [20].

In the study now presented, HDPE films having simple and well-defined stacked lamellar morphology, *either with or without* a distinct presence of row-nucleated fibril structure, have been utilized as model materials to *elucidate* and *demonstrate* the morphological changes during the process of plastic deformation. In addition, the *microscopic morphologies* developed during the deformation, as revealed by WAXS and TEM, have been related to the *macroscopic properties*, as measured by direct tensile tests. The samples for the WAXS and TEM studies were deformed to specific amount of strain according to the corresponding stress–strain curves. The mechanical properties have been explained by the development of the deformation-induced morphologies. The specific morphological features of these films also allowed us to carry out plastic deformation at different orientations with respect to the original machine direction; it is possible, therefore, not only to present a model structure–property study about the effect of orientation on the deformation morphology and the mechanical properties, but also to mimic partially the heterogeneous (position-dependent) deformation process that one encounters in the spherulitic morphology. Furthermore, with the availability of comparable materials either with or without the presence of a distinct row-nucleated fibril structure, it is also possible to understand how the mechanical property and the deformation morphology are influenced by this structure.

2. Experimental procedure

2.1. Materials

The HDPE materials used in this study were based on two resins having the same number-averaged molecular weight of 14 500 g mol^{-1} but different weight-average molecular weights of 150 000 g mol^{-1} (resin 1) and 219 000 g mol^{-1} (resin 2). The melt-extruded films of 25.4 μm thick were kindly provided by Hoechst Celanese Co. Both precursor films (melt-extruded films) and annealed films (passing the same precursor films through a heating oven at 120 °C with certain on-line speed, under about 3% tensile strain, which allows the material to stay at this temperature for about 20 min) were investigated. Films based on resin 1 are designated Pre-1 and Anl-1 for the precursor and

annealed films, respectively, and films based on resin 2 are designated as Pre-2 and Anl-2 for the precursor and the annealed films, respectively. Under similar extrusion conditions, both precursor films were quite highly uniaxially oriented. This was quantified by determination of the Hermans orientation function, f_c, for the crystalline phase using X-ray scattering, where f_c is defined as

$$f_c = \frac{1}{2}(3\langle\cos^2\theta\rangle - 1) \quad (1)$$

In Equation 1, the quantity $\langle\cos^2\theta\rangle$ represents the average value of $\cos^2\theta$, with θ being the angle between the c axis in the crystal (chain axis direction) and the machine direction (MD). The crystalline orientation function, f_c, calculated from the WAXS patterns are 0.67 and 0.71 for the Pre-1 and Pre-2 films, respectively. The corresponding annealed films (Anl-1 and Anl-2) had a slightly higher crystalline phase orientation state, with f_c increased to 0.80 and 0.81, respectively. The films based on resin 1 (both Pre-1 and Anl-1) had a stacked lamellar morphology with no sign of row structures as detected by both WAXS and TEM, whereas the films based on resin 2 (both Pre-2 and Anl-2) possessed a morphology which contained a very distinguishable amount of row-nucleated fibril structures in the matrix of stacked lamellae, the existence of the row-nucleated fibril structure having been verified by both WAXS and TEM. A detailed investigation on the morphology and orientation state of the undeformed "as-processed" HDPE films used in this study has been recently published elsewhere [71, 72].

2.2. Mechanical properties and plastic deformations

Stress–strain curves for all the HDPE films were obtained by utilizing an Instron (model 1122) at ambient conditions with a cross-head speed of 15 mm min^{-1}. Dogbone-shaped samples of size 23 mm × 8 mm were used for the stress–strain tests, and they were cut directly from the HDPE films at one of three angles, 0°, 45° and 90°, with respect to the original MD. Tensile tests were carried out for samples at each angle and are designated as 0°, 45° and 90° deformations accordingly. For each stretch angle, samples with different amounts of plastic deformation (just beyond the yield point, the break point, and one or two points between the two extremes) were obtained by stretching the dogbone samples up to specific strains as determined from the corresponding stress–strain curves. These deformed samples were then used for the WAXS and TEM studies.

2.3. Wide-angle X-ray scattering

All the WAXS experiments were performed by utilizing a Philips tabletop X-ray generator (model PW1720) with CuKα irradiation ($\lambda = 0.154$ nm) and equipped with a standard vacuum-sealed Warhus photographic pinhole camera. The instrument was operated at 40 kV and 50 mA. For undeformed films, stacks of multiple layers of films were used as samples for the experiments. For deformed (stretched) films, however, in order to minimize the effect of misalignment in stacking the samples, only single-layer films with known strains were used as samples for the experiments. In this case, the sample was stretched to a designated strain and held for a certain period of time to allow about 30% of the instantaneous stress to relax; this large amount of relaxation is due to the "springy characteristic" of these somewhat hard-elastic-type materials and it has also been noted by others [25]. The same samples were saved for later use in the TEM study.

2.4. Transmission electron microscopy

The samples for TEM studies were prepared from the stretched samples possessing a specific amount of strain. These samples were stained with chlorosulphonic acid at 60 °C for 6 h, and then they were washed with sulfuric acid and water. In order to prevent the samples from curling in the staining process, the samples were clipped between two glass plates while staining. However, the sample still shrunk somewhat after staining because of the large amount of plastic deformation that the sample had undergone within the prior mechanical test. The stained samples were embedded in an epoxy resin and cured at 65 °C overnight. The embedded samples were microtomed at room temperature with a diamond knife; thin sections of about 80 nm were collected and used for the TEM study. The microtoming direction was parallel to the stretch direction (SD). The TEM studies were performed using a Philips EM420 microscope operated at 100 kV.

3. Results

Fig. 2 shows the WAXS patterns for the Pre-1 and Pre-2 films, with the incident X-ray beam perpendicular to the MD in Fig. 2a and c and parallel to the MD in Fig. 2b and d. It can clearly be seen that the crystalline phase of the two films are well oriented along the MD, with the $(1\,1\,0)_o$ and $(2\,0\,0)_o$ reflections more or less concentrated towards the equatorial region (Fig. 2a and c), where the subscript o stands for the orthorhombic crystalline structure of HDPE (to differentiate the reflections from the monoclinic structure, as will be seen later). From Fig. 2b and d, one sees that the $(1\,1\,0)_o$ and $(2\,0\,0)_o$ reflections are quite uniformly distributed azimuthally, implying a random orientation state of the crystalline lamellae in the plane perpendicular to the MD. Therefore, the c axis (chain axis) in the crystal can be considered as quite uniaxially oriented with respect to the MD (i.e., cylindrical symmetry). In addition, the WAXS patterns for the Pre-2 films (Fig. 2c) shows highly concentrated reflections at the equator superimposed on broader or more azimuthally spread reflections of the same Bragg planes, implying the existence of a second population of highly oriented crystalline structures along the MD. No such high-intensity spots were observed for the

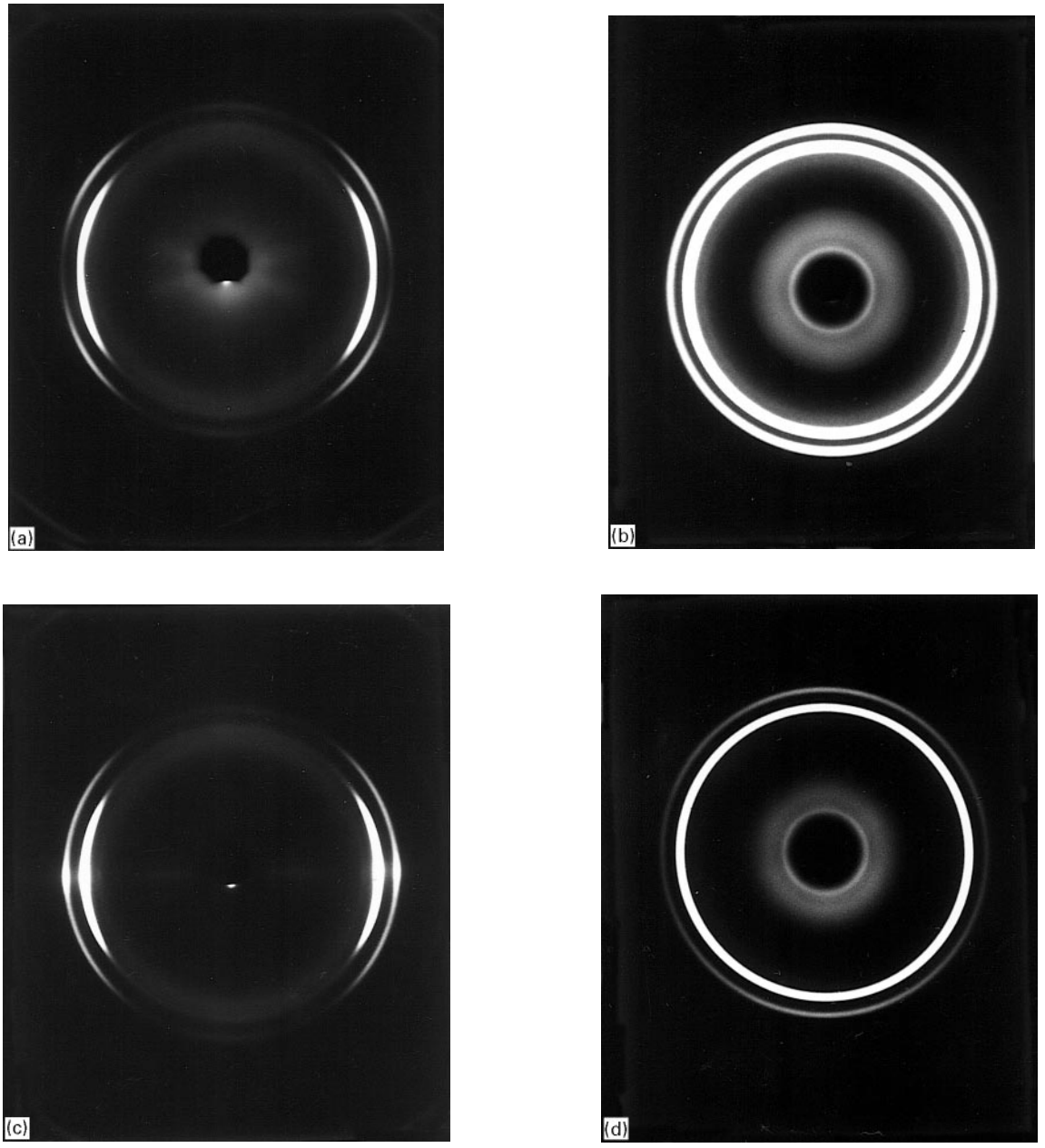

Figure 2 WAXS patterns for (a), (b) the Pre-1 and (c), (d) the Pre-2 films, for the X-ray beam (a), (c) perpendicular to the MD, and (b), (d) parallel to the MD.

Pre-1 film (Fig. 2a). It should be pointed out that the calculation of the crystalline orientation function, f_c, which is based on the azimuthal position of the reflection arcs in the WAXS patterns, did not take into account these latter azimuthally concentrated reflection spots for the R2 films.

Fig. 3a and b are transmission electron micrographs for the Anl-1 and Anl-2 films, respectively. Sample Anl-1 displays a stacked lamellar morphology while, for sample Anl-2, row-nucleated fibril structures are unambiguously revealed in addition to the well-stacked lamellae. The same kinds of morphology were observed for the respective precursor films of Pre-1 and Pre-2, except that the contrast for the precursor films is not as sharp as that for the annealed films, and the average thickness of the crystalline lamellae for the precursor films is less than that for the annealed films. The increase in lamellar thickness for the annealed films is due to lamellar thickening in the annealing process at 120 °C for about 20 min, and it has also been detected by SAXS, AFM and DSC in an earlier study [73]. The existence of the row-nucleated fibril structure observed within the R2 film morphology is responsible for the high-intensity scattering spots at the equator of the WAXS patterns for these materials, such as Fig. 2c for the Pre-2 film.

3.1. Stress–strain curves of the high-density polyethylene films

Shown in Fig. 4a and b are the stress–strain curves at the 0°, 45° and 90° deformations for the Pre-1 and Anl-1 films, respectively. The same forms of data for the Pre-2 and Anl-2 films are shown in Fig. 4c and d. These data clearly demonstrate the dramatic differences in the mechanical properties of these films, particularly those with and without row structures and

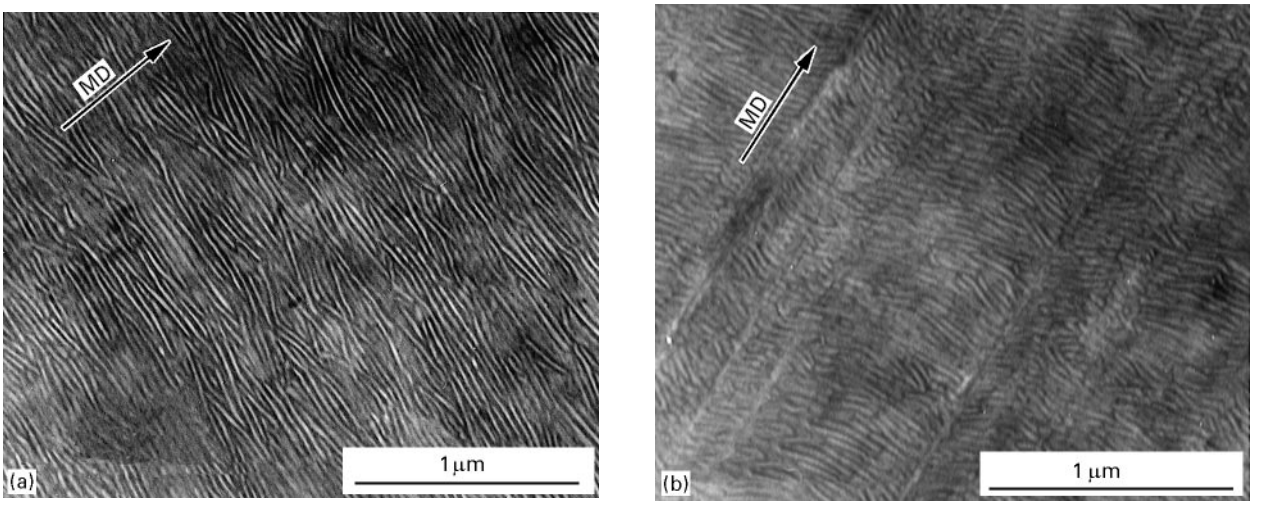

Figure 3 Transmission electron micrographs for (a) the Anl-1 and (b) the Anl-2 films.

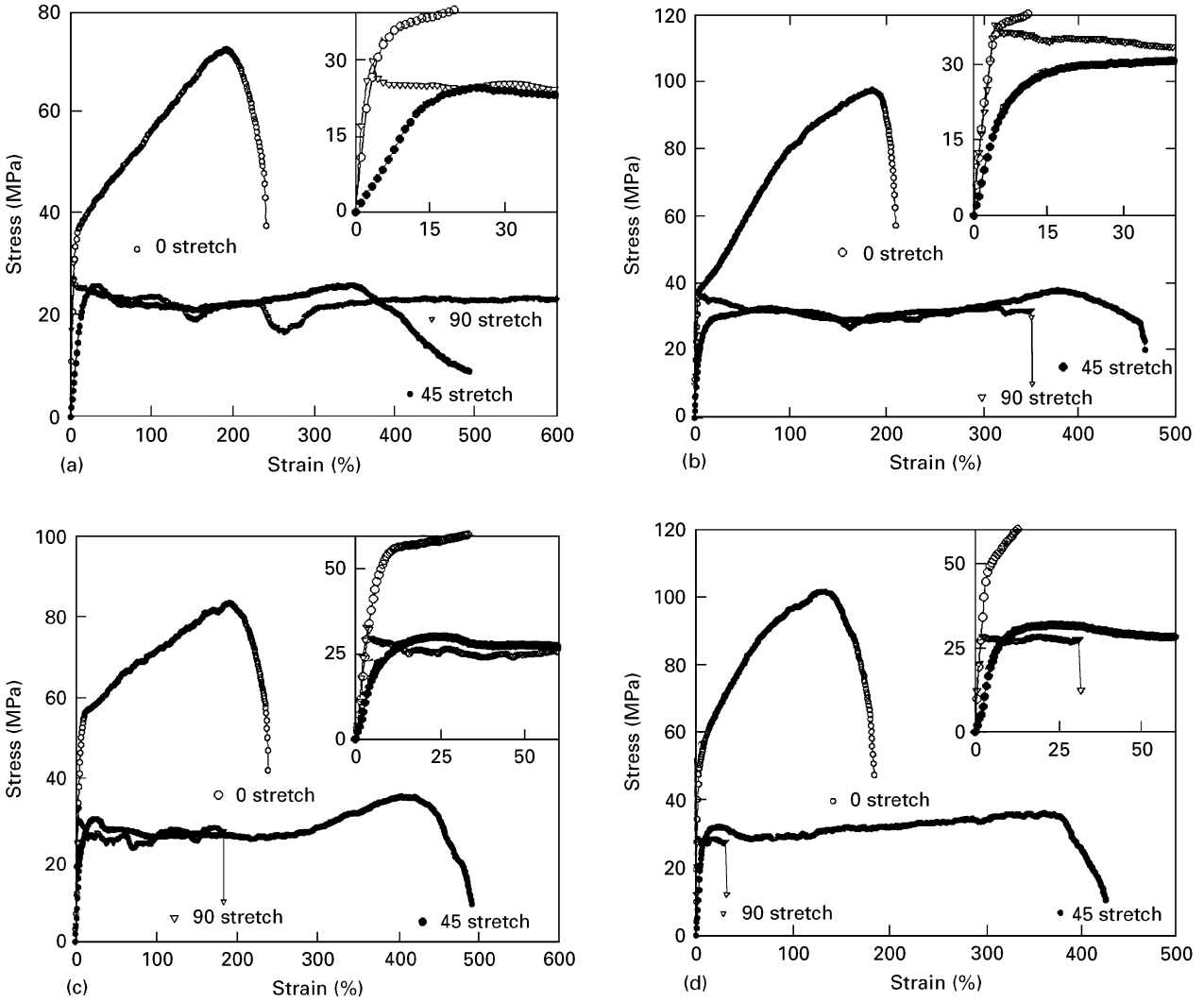

Figure 4 Stress-strain curves for (a) the Pre-1, (b) the Anl-1, (c) the Pre-2 and (d) the Anl-2 films.

those with or without thermal annealing. The properties of Young's modulus, E, yield stress, σ_y, and strain, ε_y, cold-drawn stress, σ_d, and strain, ε_d, break stress, σ_b, and strain, ε_b, determined from these curves are listed in Table I and will be discussed later.

For the 0° deformation, after yielding, which *in this case is denoted by where a deviation from initial linearity* occurs, all the samples displayed a significant degree of strain hardening, indicated by the large positive slopes following yielding. That is, no neck

TABLE I Values of Young's modulus, E, yield stress, σ_y, and strain, ε_y, cold-drawing stress, σ_d, breaking stress, σ_b, and strain, ε_b, for the four HDPE films investigated

Property (units)	Orientation (deg)	Value for the following films			
		Pre-1	Anl-1	Pre-2	Anl-2
E (MPa)	0	530	920	892	1500
	45	290	430	395	460
	90	750	940	1040	1600
σ_y (MPa)	0	35	36	55	56
	45	23	27	28	31
	90	30	35	33	28
ε_y (%)	0	8	6	10	8
	45	14	9	3	11
	90	3	3	15	3
σ_d (MPa)	0	—	—	—	—
	45	22	32	26	28
	90	22	32	26	27
σ_b (MPa)	0	72	98	82	102
	45	>26	>38	>38	>35
	90	>24	32	30	27
ε_b (%)	0	220	185	170	125
	45	350	>380	>410	>360
	90	>960	350	185	32

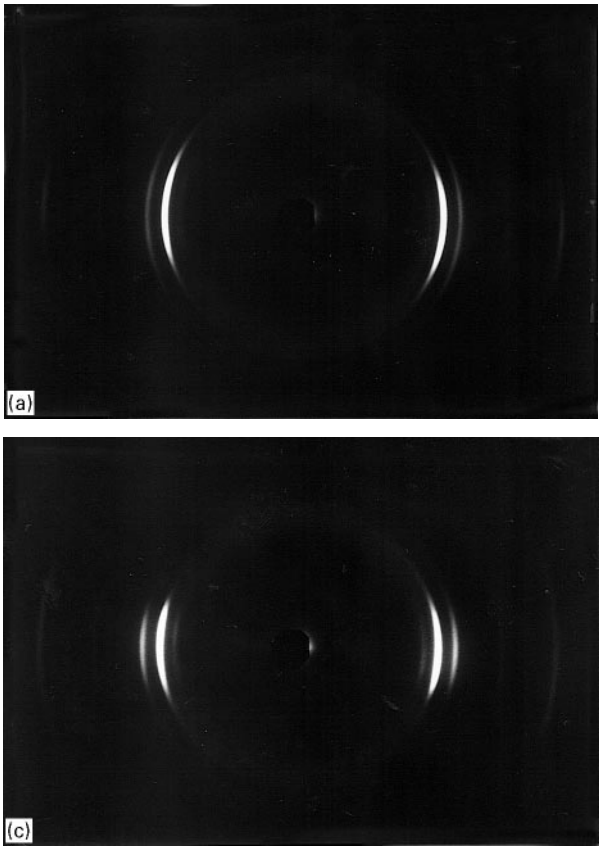

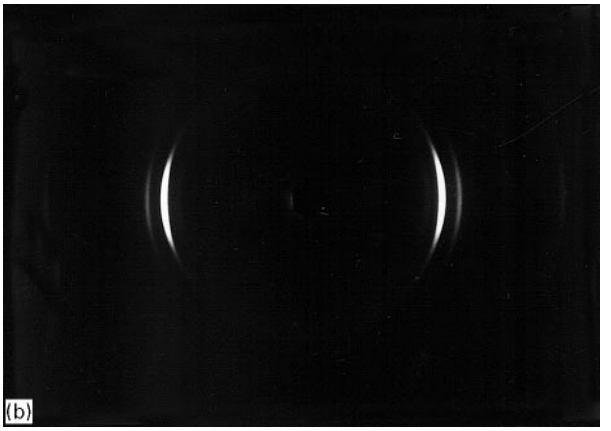

Figure 5 WAXS patterns for the Pre-1 film for the 0° deformation at (a) $\varepsilon = 15\%$, (b) $\varepsilon = 100\%$ and (c) $\varepsilon = 180\%$. Both the MD and the SD are vertical.

formation was found over the entire deformation. However, strain whitening was found in the neighbourhood of yielding for all the samples. For the 90° deformation, all samples displayed a very different yielding style, *a sharp* "*conventional*" *yield peak*, compared with the case of 0° deformation, and necked at very early stages of the deformation (less than 5% strain); they then underwent cold drawing to different amount of strains for different samples. Eventually, the samples broke in a "brittle" fashion with no or a slight amount of strain hardening. Also noticed is the uneven feature of these stress–strain curves in the drawing region, particularly for the Pre-1 and Pre-2 films. The 45° deformation showed a behaviour which is similar to those of unoriented semicrystalline polymers with a spherulitic morphology, i.e., a well-defined local yielding maximum, strain softening, cold drawing and finally strain hardening before failure. Necking took place by shear at about 45° to the SD. At the last stage of deformation, the samples failed by tearing slowly at the end of the clamps, shown as downward tails at the end of the respective stress–strain curve.

3.2. Wide-angle X-ray spectroscopy results

Fig. 5a, b and c are the WAXS patterns for the Pre-1 films deformed at the 0° stretch to strains of 15%,

100% and 180%, respectively. Comparing these WAXS patterns with that pattern from the respective undeformed sample (Fig. 2a), it can be seen that there is a trend to increase the orientation state of the crystalline phase, manifested by the more concentrated $(1\,1\,0)_o$ and $(2\,0\,0)_o$ scattering intensities in the equatorial region. Additionally, it can also be seen, from Fig. 5c, that there is an extra weak reflection developed inside the $(1\,1\,0)_o$ scattering, which is the $(1\,0\,0)_m$ of the monoclinic crystalline phase of HDPE due to the martensitic phase transformation. Fig. 6a, b and c are the WAXS patterns for the Pre-2 films deformed at the 0° stretch to strains of 15%, 50% and 120%, respectively. In addition to the same trend showing an increase in the orientation state of the crystalline phase in the process of plastic deformation, the decrease (Fig. 6b) and disappearance (Fig. 6c) of the intense scattering spots at the equator were also clearly noticed. Interestingly, the existence of the $(1\,0\,0)_m$ reflection is not observed at the highest strain of 120%.

For the 90° stretch, the samples necked immediately at about 3–5% strain, and what followed was the expansion of the neck along the entire length direction of the sample. It was expected that samples in the necked region should essentially possess the same kind of morphology. The WAXS patterns for the 90° stretch for the Pre-1 and Pre-2 films are shown in Fig. 7a and b, respectively; they show basically the same general highly oriented state of the crystalline phase with respect to the SD, *which is now perpendicular to the original MD*. It is also noted that the monoclinic crystalline phase exists in the necked region.

Fig. 8 and Fig. 9 present the morphological changes for the 45° stretch for the Pre-1 and Pre-2 films, respectively. For the Pre-1 film, at 30% strain (Fig. 8a), there was no significant change in crystalline orientation that has been found by WAXS. However, at a strain of 60% (Fig. 8b), the WAXS patterns became asymmetric, giving the $(1\,1\,0)_o$ reflections in Fig. 8b. The crystalline orientation state in this case is not very different from that at 30% strain, judged by the "spreading" of the $(1\,1\,0)_o$ reflection, but the

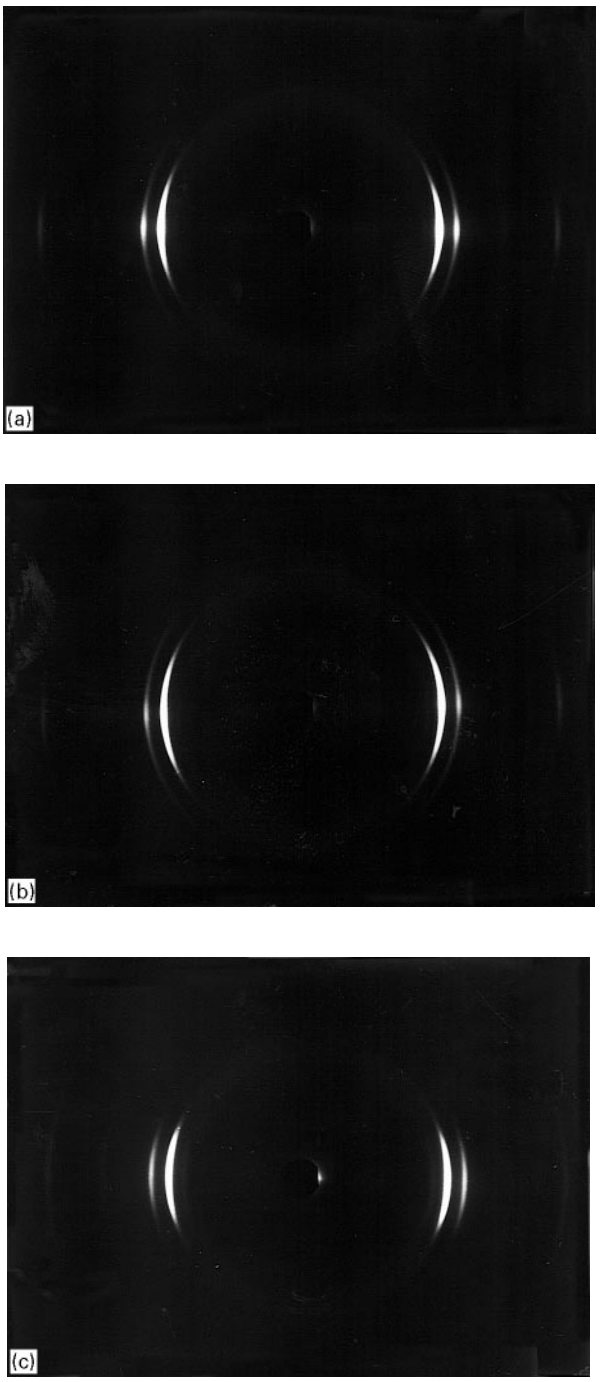

Figure 6 WAXS patterns for the Pre-2 film for the 0° deformation at (a) $\varepsilon = 15\%$, (b) $\varepsilon = 50\%$ and (c) $\varepsilon = 120\%$. Both the MD and the SD are vertical.

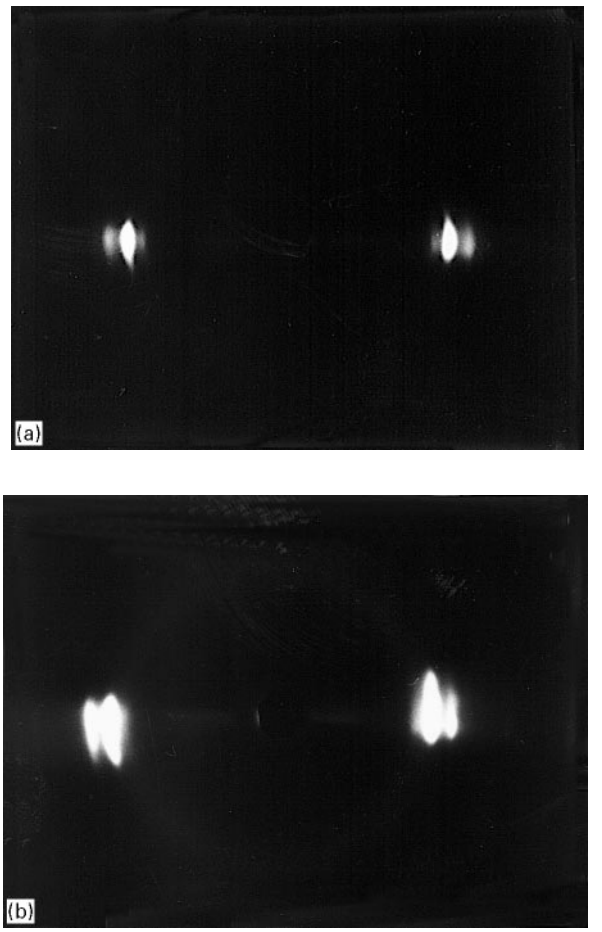

Figure 7 WAXS patterns for (a) the Pre-1 and (b) the Pre-2 films for the 90° deformations. The original MD is horizontal, and the SD is vertical.

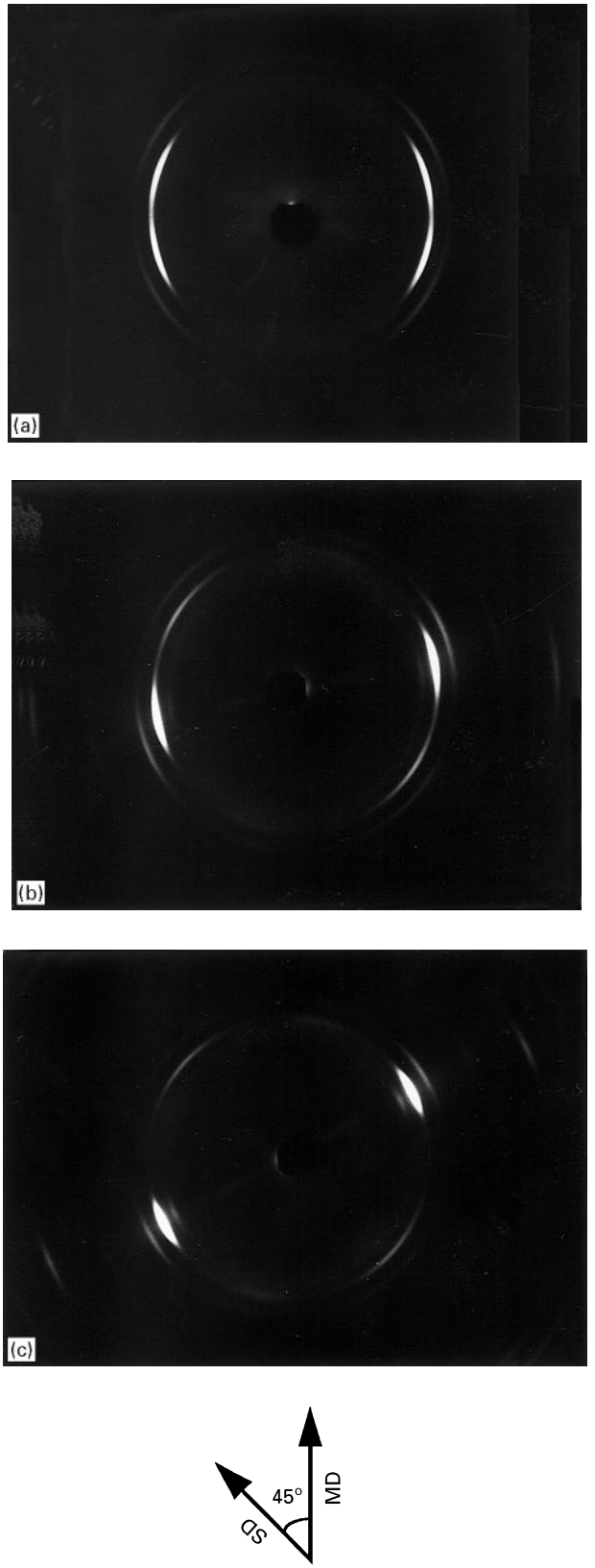

Figure 8 WAXS patterns for the Pre-1 film for the 45° deformation at (a) $\varepsilon = 30\%$, (b) $\varepsilon = 60\%$ and (c) $\varepsilon = 180\%$. Both the SD (stretch direction) and the MD (extrusion direction) are shown in the figure.

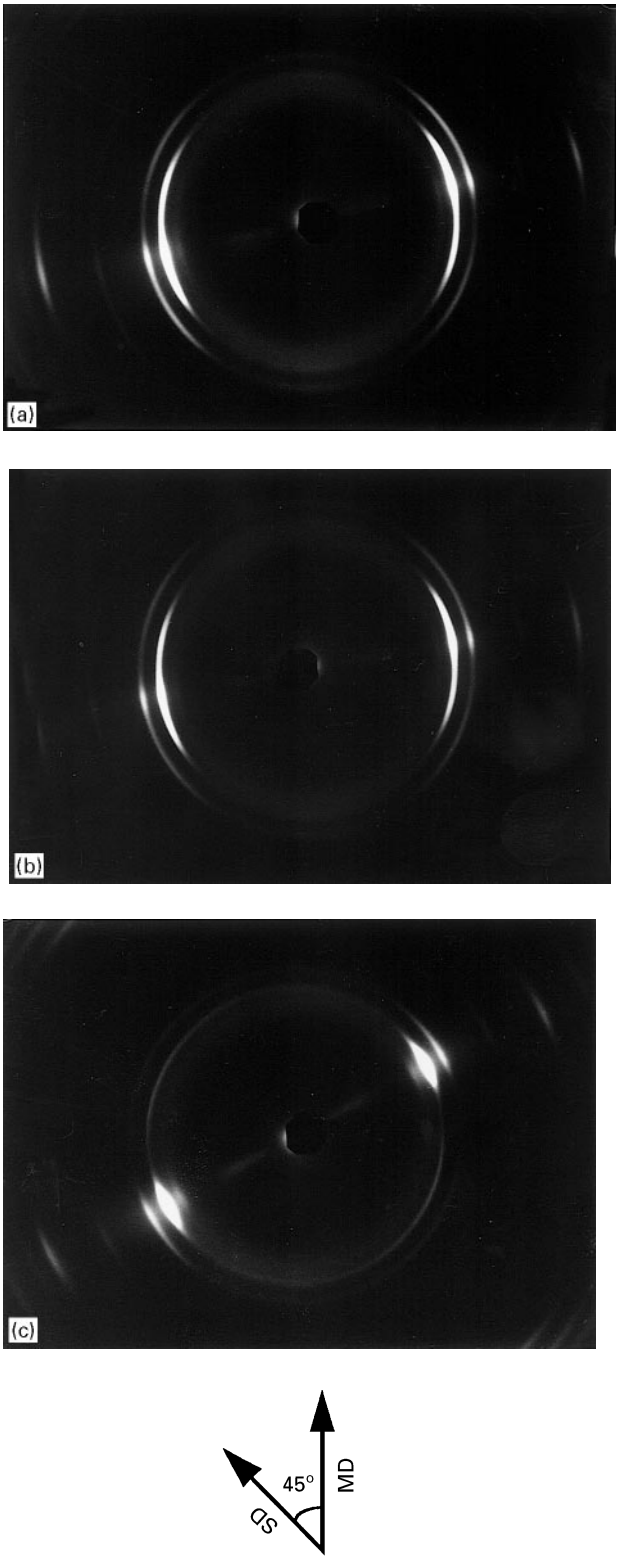

Figure 9 WAXS patterns for the Pre-2 film for the 45° deformation at (a) $\varepsilon = 25\%$, (b) $\varepsilon = 50\%$ and (c) $\varepsilon = 150\%$. Both the SD (stretch direction) and the MD (extrusion direction) are shown in the figure.

rotation of crystalline lamellae towards the SD is suspected; such a rotation can be speculated by a change in the angular position of the $(1\,1\,0)_o$ reflections with respect to the SD (as shown in Fig. 8b). At a further strain of 180% (Fig. 8c), a new symmetric scattering pattern with respect to the SD is now established. Again, the monoclinic crystalline structure was observed for the sample with 180% strain. A similar trend of the formation of a new orientation state along the SD was also observed for the Pre-2 film, as shown in Fig. 9a, and in this case the rotation of crystalline lamellae with respect to the SD, based on the above conjecture, took place at the early stages of the deformation (Fig. 9a).

3.3. Transmission electron microscopy results

Fig. 10a and b present the transmission electron micrographs for the Anl-1 and Anl-2 films at the 0° deformation with individual strains of 100% and 50%, respectively. For the stacked lamellar morphology (the Anl-1 film), broken blocks of the crystalline lamellae are observed (Fig. 10a) while, for the row containing morphology (the Anl-2 film), the localized break-up of row-nucleated fibril structure is observed (shown by the arrows in Fig. 10b). It can be seen that the crystalline lamellae in the deformed samples (Fig. 10) are not as well defined as those in the undeformed samples (Fig. 3), probably because of the large amount of defects in the crystalline lamellae due to plastic deformation. Samples with smaller amounts of strains (just beyond the yield point) were also investigated, but no significant changes could be seen by TEM, possibly partially because of some sample shrinkage during the staining treatment.

Fig. 11a and b present the dramatic morphological changes at the sharp boundary of the necks for the

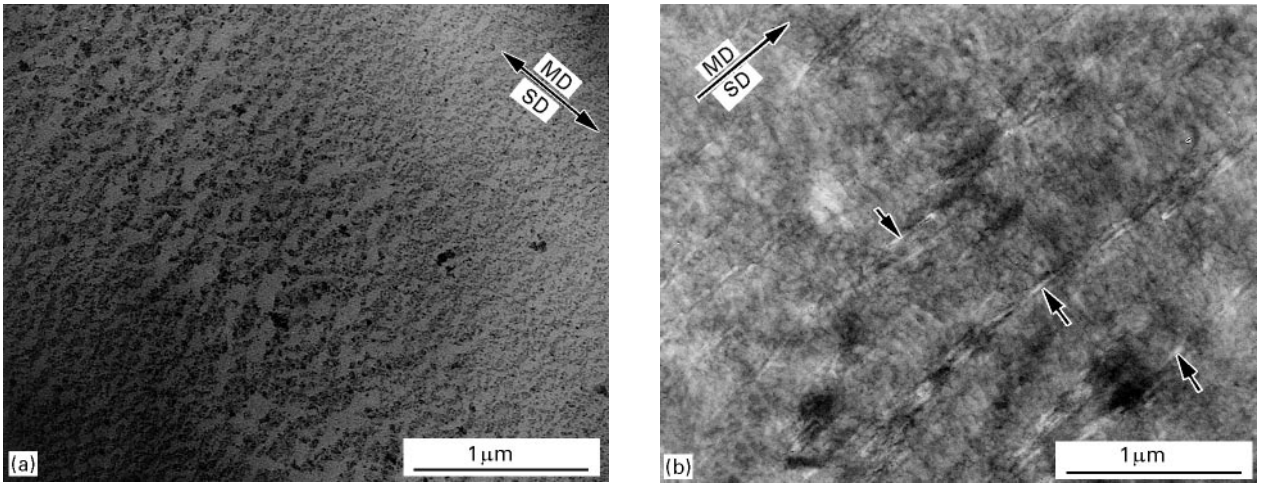

Figure 10 Transmission electron micrographs for (a) the Anl-1 film for the 0° deformation at $\varepsilon = 100\%$ and (b) the Anl-2 film for the 0° deformation at $\varepsilon = 50\%$. The arrows shown in this figure indicate broken row-nucleated fibril structures.

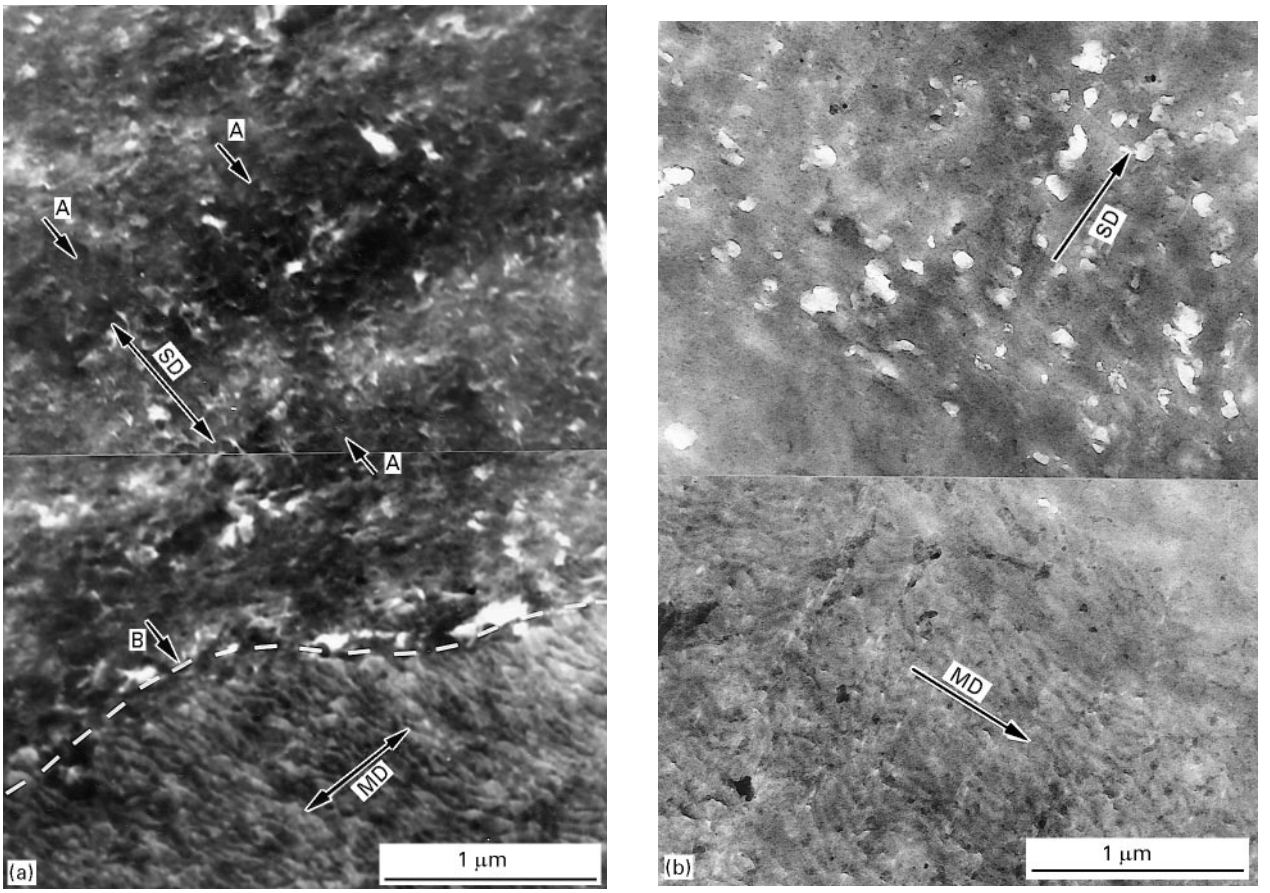

Figure 11 Transmission electron micrographs showing the boundary of necked and un-necked regions for (a) the Anl-1 and (b) the Anl-2 films. Arrows A in (a) point to short broken white lines which indicate the presence of microfibril crystalline materials, and arrow B points to a broken line which follows the sharp boundary of the necked and un-necked regions.

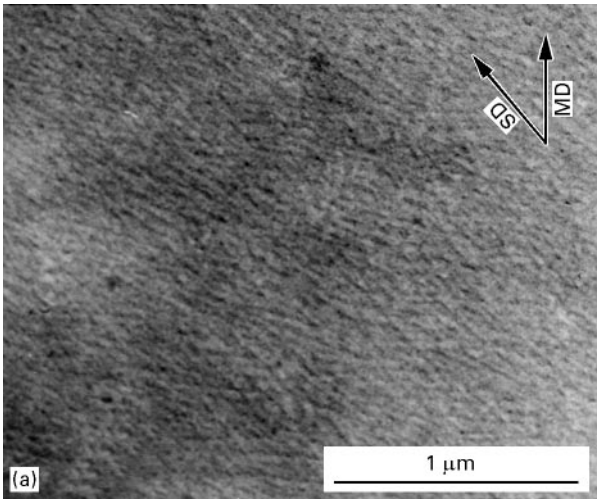

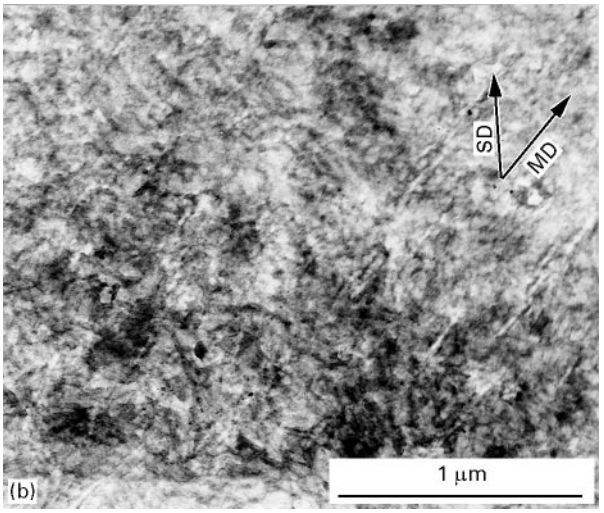

Figure 12 Transmission electron micrographs for the 45° deformation for (a) the Anl-1 film at $\varepsilon = 25\%$ and (b) the Anl-2 film at $\varepsilon = 30\%$.

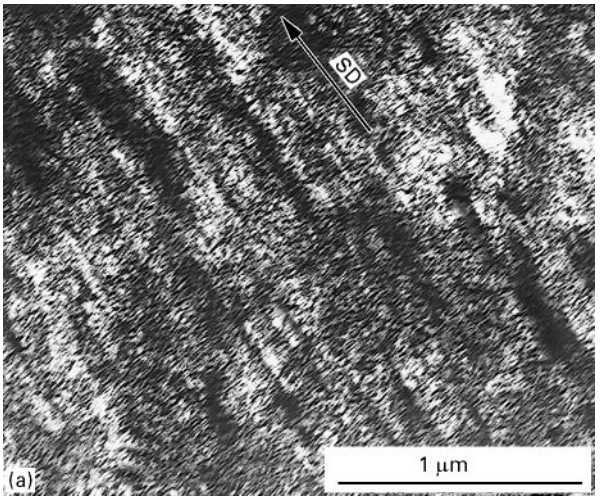

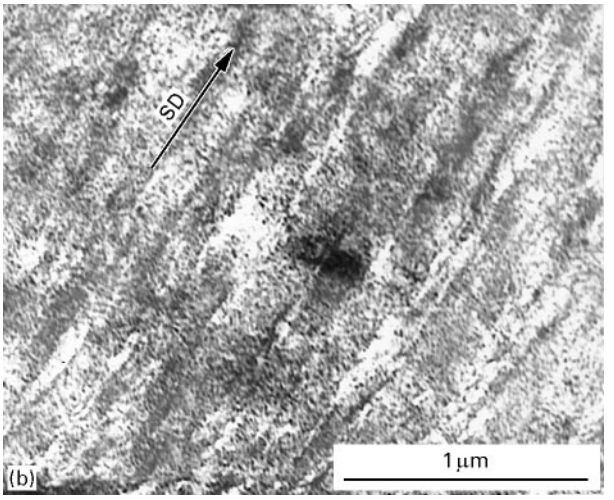

Figure 13 Transmission electron micrographs for the 45° deformation for (a) the Anl-1 film at $\varepsilon = 180\%$ and (b) the Anl-2 film at $\varepsilon = 150\%$.

Anl-1 and Anl-2 films, respectively, at the 90° deformation. The top and bottom portions of each of these micrographs represent the necked and un-necked regions, respectively. There are also transition regions between the necked and un-necked regions, but the detailed features cannot be well resolved. For the Anl-1 film (Fig. 11a), the un-necked region shows the original stacked lamellar morphology oriented along the MD, while the necked region displays considerable void fraction and broken white lines (shown by arrows A in Fig. 11a) oriented along the SD; these lines may be an indication of a microfibril crystalline phase. For the Anl-2 film (Fig. 11b), the un-necked region shows the crystalline lamellae and the row structures along the SD while, in the necked region, more and larger voids along the SD are seen without the presence of the broken white lines. The crystalline lamellae in the un-necked regions in Fig. 11a and b do not look the same as those in Fig. 3 since the microtoming direction in this case is *perpendicular* to the MD. Additionally, the plastic deformation can also influence the lamellar morphology, as mentioned in the case of the 0° deformation.

Fig. 12a and b are transmission electron micrographs for the Anl-1 and Anl-2 films, each stretched at a 45° deformation. For the Anl-1 film (Fig. 12a), at a low strain (about 25%), "shear-banding"-type features are observed, which implies lamellar shear deformation. However, for the Anl-2 film (Fig. 12b), localized break-up of the row structures is noted. Again, the crystalline lamellae deteriorate, and the morphology observed by TEM becomes less and less well defined as the deformation proceeded. Finally, at a strain of 200%, a highly oriented morphology was observed for both the Anl-1 and the Anl-2 films (Fig. 13a and b). However, the expected microfibril crystalline structure was not observed, and other fine textures in these micrographs cannot be addressed unambiguously, owing to the absence of the original MD. However, by using the knife marks on the samples and/or samples edges as an indication of the SD, the rotation of the crystalline lamellae can indeed be distinctly inferred.

4. Discussion

4.1. Young's modulus at different orientations

The variation in mechanical properties listed in Table I can be explained by the specific *initial*

morphologies and also those *developed* during the deformation processes of these HDPE films. We shall first address Young's modulus, since it depends on the low-deformation elastic behaviour of the materials. Structural models for the HDPE films will be established according to the morphological features of the films and will also be utilized in the discussion of the other properties associated with the plastic deformation of the materials.

For the films based on resin 1 (Pre-1 and Anl-1), the crystalline lamellae are uniaxially oriented with the lamellar normal preferentially aligned parallel to the MD. Therefore, as a first approximation, these specific materials based on resin 1 can be considered as a "laminated composite" of a hard crystalline phase and a soft amorphous phase stacked along the MD. At the 0° deformation, the material can be considered as the composite being deformed in an iso-stress case, i.e., the crystalline phase and the amorphous phase are deformed in series; therefore the modulus is dominated by that of the soft amorphous phase. On the other hand, at the 90° deformation, the material can be considered as the composite being deformed in an iso-strain case, i.e., the crystalline phase and the amorphous phase are deformed in parallel; therefore the modulus is dominated by that of the hard crystalline phase. Thus, although the modulus of the *crystalline phase* (*lamellae*) at the 90° orientation (perpendicular to the chain direction) is much less than that at the 0° orientation (more parallel to the chain direction), the modulus for the sample at the 90° orientation is *higher* than that for the sample at the 0° orientation. As for the 45° deformation, since there is a maximum resolved shear stress in the plane of the crystalline lamellae, interlamellar shear is the most probable deformation event, and this results in an even smaller modulus at this particular orientation than those for the 0° and 90° deformations.

For the films based on resin 2 (Pre-2 and Anl-2), in addition to the uniaxially oriented stacked crystalline lamellae, many row-nucleated fibril structures also exist, as observed directly by TEM. From previous studies concerning HDPE films having a shish-kebab morphology, three different structural models have been proposed, i.e., interlocking lamellae [74], fibre-reinforced composite [75] and crystalline network [76]. We select the fibre-reinforced composite model for use in this study, since it best represents the structural features of these materials shown by the transmission electron micrograph in Fig. 3b; additionally, this model is closely coupled to the laminated composite model proposed for the stacked lamellar morphology.

The row structures in the films based on resin 2 serve as reinforcement fibres having a large aspect ratio (Fig. 3b) in the MD, and this gives rise to the higher modulus at the 0° deformation, compared with that for the films based on resin 1 (the Pre-2 film versus the Pre-1 film as well as the Anl-2 film versus the Anl-1 film). However, at 90° deformation, the strengthening effect of the row structures (fibre reinforcements) is not as effective as for the 0° deformation; therefore, the increase in Young's modulus at this orientation is not as significant as that for the 0° deformation, again comparing Young's modulus for the Pre-2 film with that for the Pre-1 film and comparing Young's modulus for the Anl-2 film with that for the Anl-1 film. For the 45° deformation, although limited by the existence of the row structures, lamellar shear still dominated in the initial stage of the deformation, and this gives rise to the lowest modulus of the three deformation orientations. We realize that the above analysis is somewhat *qualitative* and may not be fully correct owing to the small difference in the crystalline orientation state (f_c values) possessed by these two films.

4.2. Plastic deformation morphologies at different orientations

Other properties, namely, yield stress, σ_y and strain, ε_y, cold-drawn stress, σ_d, and strain, ε_d, and break stress, σ_b, and strain, ε_b, are related to the plastic deformation behaviour of the materials. As can be seen from the stress–strain curves in Fig. 4, the mechanical behaviour of the films strongly depended on the orientation of the deformation, and they will be discussed separately below. Other factors, such as molecular weight distribution, thermal annealing and orientation state of the crystalline phase, will also certainly affect these properties; however, they will not be discussed in this report.

4.2.1. 0° deformation

Considering the "laminated composite" model proposed earlier for films based on resin 1, its deformation along the MD would occur by lamellar separation. Such a deformation mechanism can be justified by the appearance of strain whitening for samples stretched along the MD and the disappearance of such a phenomenon for relaxed samples upon removal of the stress. Similar statements have been made from the deformation studies on other hard-elastic polyethylene [25] and polypropylene [77], which have a similar morphology to the resin 1 samples deformed along the MD. Lamellar separation cause crystalline lamellae to "open up" or splay, and this results in the strain whitening shown by all the samples. As the deformation proceeded, the crystalline lamellae have to be deformed to generate higher strains, and this promotes yielding of the sample. Since the *c* axis in the crystal is more or less oriented along the stress direction (MD), chain slip is the dominant deformation mode for the crystalline phase, especially [1 0 0] chain slip. The slip of the crystalline phase also causes the large degree of strain hardening, as shown in the stress–strain curves.

As mentioned earlier, chain slip can be achieved by either fine slip or coarse slip; however, the physical process for both types of slip is the same, i.e., sliding between chains in polymer crystals. For fine slip, the sliding is between chains in the same crystal unit cell whereas, for the coarse slip, the sliding is believed to be between chains at the boundary of the mosaic blocks within the crystalline lamellae [78]. The result from

TEM observations (Fig. 10a) suggested that coarse slip has taken place, and by doing this the crystalline lamellae were fragmented into much smaller crystal blocks, which probably originate from the mosaic blocks within the crystalline lamellae. The same observation of coarse-slip-induced fragmentation of large crystalline lamellae has also been made by others [14].

As for the films based on resin 2, the existence of row-nucleated fibril structure obviously affected the initial stage of the deformation, as shown by the higher values of Young's modulus. However, the basic plastic deformation processes described above were not expected to change. Once the yield point was passed, the row structures began to break up gradually at certain localized points (see Fig. 10b), indicating that the fibril structure is not likely to be of a complete extended-chain-type crystalline phase [79]. The strengthening effect on the further plastic deformation became less and less. From the stress–strain curves, the films with and without row structures had similar behaviours from yield point to break point, i.e., *the degree of strain hardening* (*slope of the curve*) *for the Pre-1 and Pre-2 films and for the Anl-1 and Anl-2 films were similar*.

4.2.2. 90° deformation

At this orientation, since the *c* axis (chain axis) in the crystalline lamellae was more or less perpendicular to the direction of the applied stress (SD), the deformation on the level of the crystalline lamellae and amorphous layers, via lamellar separation, lamellar shear and lamellar rotation, was significantly limited. Therefore, the samples yielded sharply after a small amount (3–5%) of iso-strain elastic deformation of the crystalline phase and amorphous phase, and what followed was the localized break-up (decrystallization) of the crystalline lamellae, by transverse slip in the crystal. During the decrystallization process, polymer chains are pulled out of the crystalline lamellae and realigned and recrystallized parallel to the SD, which is perpendicular to the original MD. The pull-out of the chains is basically a cold-drawing process and, therefore, it occurred as a horizontal plateau in the stress–strain curves at the 90° deformation.

However, the films based on the two resins behave very differently. As shown in the stress curves, those with a stacked lamellar morphology showed a large degree of cold drawing, while those with a row morphology showed only a very limited amount of cold drawing. This difference can be explained by the different kinds of morphology developed for the respective films, as revealed by the transmission electron micrographs shown earlier in Fig. 12. For the stacked lamellar morphology, there is no rotation of the crystalline lamellae in the un-necked region, and the chain pull-out allows a deformation strain as high as 1000% for the Pre-1 film (shown by the stress–strain curve). The same lamellar break-up via chain pull-out has also been noted by other workers [18, 19]. However, it was seen that the row-nucleated fibril structure in the un-necked region was oriented along the SD, and such a rotation of the shish structure has also been reported by Brady and Thomas [24] based on TEM studies on specially prepared ultrathin and ultradrawn HDPE films. It was speculated that the rotation of the row-nucleated fibril structure is very limited; thus the cold-drawn strain induced was also very small. Hence, within this context, it seems that the crystalline network model for the row morphology serves better to explain the constrained rotation of the row-nucleated fibril structures and associated stacked lamellae.

4.2.3. 45° deformation

As mentioned earlier, interlamellar shear was the dominate deformation mode at the early stage of the deformation at this orientation. Also this corresponded to a larger observed yield strain and lower yield stress, compared with the deformations at the 0° and 90° orientations. To accommodate the lamellae shear, however, chain slip, either fine or coarse, takes place through the sliding of tie chains, and this corresponds to the yielding of the crystalline phase. A closer examination of the stress–strain curves at the 45° orientation indeed showed a hint of double yielding. Double yielding has been reported previously for HDPE [80, 81], and in that case the two yield points were speculated to originate from lamellar shear and the subsequent deformation of the crystalline phase, respectively.

In the process of yielding, lamellar rotation occurred as a result of lamellar shear and/or chain slip, and the reorientation of polymer chains towards the SD, which is 45° away from the original MD, as shown by the WAXS patterns (Figs 8 and 9). At this stage of the deformation, crystalline lamellae began to break up owing to the competitive constraint between lamellar shear and chain slip, as also proposed by Bevis and Crellin [63]. The break-up of the crystalline lamellae is essentially a cold-drawing process by chain slip within the crystalline lamellae, in contrast with the pull-out of chains in the case of the 90° deformation. Indeed, the stress–strain curves showed a horizontal plateau in this region of strain. It is interesting to note that the cold-drawing stresses for the same sample at these two stretch orientations (45° and 90°) were almost identical. However, the cold-drawing strains at the 45° deformation seemed to be higher than at the 90° deformation (except for the pre-1 film), owing to a greater degree of chain slip rather than chain pull-out.

4.3. Plastic deformation of spherulitic morphology

Because of the complex arrangement of the crystalline phase and amorphous phase in this particular crystal texture, the deformation of a spherulite is highly heterogeneous, as already depicted earlier in Fig. 1. At the polar region, the crystalline lamellae are deformed as in the 90° deformation while, at the equatorial region, the crystalline lamellae are deformed as in the 0° deformation; the inclined region in the spherulite resembles the 45° deformation. Using the stress–strain curves in Fig. 4 as a general guide, it can be conjectured that the break-up of a spherulite occurs first in

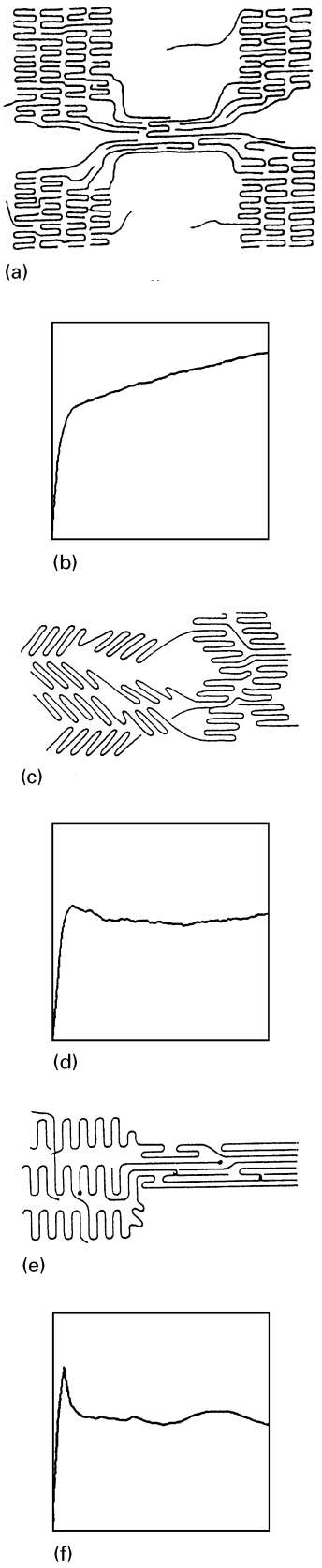

Figure 14 Schematic drawings that show the molecular mechanisms and corresponding stress–strain curves for the stacked lamellar morphology under the 0°, 45° and 90° deformations. (a), (c) and (e) are from [14], from [2] and from [19], respectively, and (b), (d) and (f) are drawn on the basis of the stress–strain curves in Fig. 4a.

the polar region since the 90° deformation results in lamellar break-up at the smallest strain level, followed by the splaying of the equatorial region where the 0° deformation lamellar separation causes the materials to yield by coarse slip with the formation of craze, and by the distortion of the inclined region in which the 45° deformation induces lamellar shear and lamellar rotation. The above argument is supported by direct observations from polarized optical microscopy [16] and SEM [13, 58, 82].

However, large amounts of intercrystalline links and geometrical constraints are expected between crystalline lamellae within a spherulite [83] ; therefore, the orientation dependence of the plastic deformation in different regions of the spherulite is not as sharply different as those noted here for the HDPE films with stacked lamellar textures. Also, because of the often prevalent twisting of the crystalline lamellae during the growth of the spherulite [84], lamellar rotation (untwisting) is believed to take place initially in all the regions of the spherulite [16], and this results in a small amount of initial homogeneous (pseudoaffine) deformation of the spherulite.

The above discussion can be summarized by the schematic drawings in Fig. 14, showing the deformation at the three angles for the stacked lamellar morphology. For the 0° deformation (Fig. 14a [14]), lamellar separation induces the fragmentation of the stacked lamellae by chain slip, and this process is shown as a strong strain-hardening event in the corresponding stress–strain curve (Fig. 14b). For the 90° deformation, plastic strain is generated by lamellar break-up via chain pull-out (Fig. 14e [19]), and this event corresponds to a large amount of cold drawing as shown in Fig. 14f. For the 45° deformation, the mechanisms may include many molecular processes such as chain slip, chain tilt and lamellar break-up (Fig. 14c [2]), and the corresponding stress–strain curve is also somewhat between those for the 0° and 90° deformation (Fig. 14d). Hence, while this deformation is more complex, *it is probably more "generic" of that observed for semicrystalline polymers having a spherulitic morphology when deformed above its glass transition temperature.*

5. Conclusions

By carrying out plastic deformation studies on HDPE films having well-defined stacked lamellar morphology, with and without row-nucleated fibril structures, we have shown that the mechanical properties and morphological changes are strongly dependent on the orientation of the deformations. By comparing the mechanical property obtained from tensile tests and the deformation morphology from WAXS and TEM at specific strain, a model structure–property investigation has been presented.

Stretching parallel to the MD results in lamellar separation and is followed by break-up of the crystalline lamellae via chain slip in coarse fashion. The existence of the row-nucleated fibril structure increases Young's modulus in this particular orientation, but the strengthening effect is reduced as deformation proceeds, owing to the localized break-up of the row structures. Stretching perpendicular to the MD causes the crystalline lamellae to break up or to rupture by chain pull-out. The effect of row-nucleated

fibril structure is to alter pull-out of the chains into the rotation of the row-nucleated fibril structure, and this results in a large amount of cold drawing for the stacked lamellar morphology and a small amount of cold-drawing for those with distinct row-nucleated fibril structures. When the stretching is between the above two extremes, lamellar shear is the dominate initial deformation mode, followed by chain slip which can eventually cause lamellar break-up. The row-nucleated fibril structure does not display a major influence at this particular orientation.

Acknowledgement

The authors would like to thank Hoechst Celanese Co. for providing the melt-extruded HDPE films for this study.

References

1. W. G. PERKINS and R. S. PORTER, *J. Mater. Sci.* **12** (1977) 2355.
2. A. PETERLIN, *Colloid Polym. Sci.* **265** (1987) 357.
3. R. S PORTER and L. H. WANG, *J. Macromolec. Sci. Macromol. Chem. Phys. C*, **35** (1995) 63.
4. I. L. HAY and A. KELLER, *J. Mater. Sci.*, **1** (1966) 41.
5. *Idem.*, *ibid.* **2** (1967) 538.
6. A. COWKING, J. G. RIDER, I. L. HAY and A. KELLER, *ibid.* **3** (1968) 646.
7. J. J. POINT, G. A. HOMES, D. GEZOVICH and A. KELLER, *ibid.* **4** (1969) 908.
8. L. LIN and H. S. ARGON, *ibid.* **29** (1994) 294.
9. I. M. WARD (ed.), "Structure and properties of oriented polymers" (Applied Science, Barking, Essex, 1975).
10. H. VAN DER WERLL and A. J. PENNINGS, *Colloid Polym. Sci.* **269** (1991) 747.
11. J. M. SHULTZ, *Polym. Engng Sci.* **24** (1984) 770.
12. R. J. SAMULES, "Structured polymer properties" (Wiley, New York, 1974).
13. I. L. HAY and A. KELLER, *Kolloid Z. Z., Polym.* **204** (1965) 43.
14. T. TAGAWA and K. OGNRA, *J. Polym. Sci., Polym. Phys. Edn* **18** (1980) 971.
15. J. LIN and Y. LEE, *J. Mater. Sci.* **28** (1993) 6496.
16. M. ABOULFARAJ, C. G'SELL, B. ULRICH and A. DAHOUM, *Polymer* **36** (1995) 731.
17. T. JUSKA and I. R. HARRISON, *Polym. Engng Rev.* **2** (1982) 13.
18. R. M. GOHIL and J. PETERMANN, *J. Polym. Sci., Polym. Phys. Edn* **17** (1979) 52.
19. J. PETERMANN, W. KLUGE and G. LEITER, *ibid.* **17** (1979) 1043.
20. J. PETERMANN, R. M. GOHIL, M. MASSUD and D. GORITZ, *J. Mater. Sci.* **17** (1982) 100.
21. R. M. GOHIL and J. PETERMANN, *J. Polym. Sci., Polym. Phys. Edn* **17** (1979) 525.
22. W. W. ADAMS, D. YANG and E. L. THOMAS, *J. Mater. Sci.* **21** (1986) 2238.
23. J. M. BRADY and E. L. THOMAS, *J. Polym. Sci., Polym. Phys. Edn* **26** (1988) 2398.
24. *Idem., J. Mater. Sci.* **24** (1989) 3311.
25. B. CAYROL and J. PETERMANN, *J. Polym. Sci., Polym. Phys. Edn* **12** (1974) 2169.
26. G. H. MICHLER, *Colloid Polym. Sci.* **270** (1992) 627.
27. H. J. KESTENBACH and J. PETERMANN, *Polymer* **24** (1994) 5217.
28. K. D. JANDT, M. BUHK, M. J. MILES and J. PETERMANN, *ibid.* **35** (1994) 2459.
29. S. HILD, W. GUTMANNSBAUER, R. LUTHI, J. FUHRMANN and H. J. GUNTHERODT, *J. Polym. Sci.* **34** (1996) 1953.
30. H. SCHONBERR, G. J. VANSCO and A. S. ARGON, *Polymer* **36** (1995) 2115.
31. P. ALLAN and M. BEVIS, *Phil. Mag. A* **35** (1977) 405.
32. J. PETERMANN and R. M. GOHIL, *Polymer* **20** (1979) 596.
33. G. L. WILKES, *ibid.* **6** (1971) 1465.
34. P. B. BOWDEN and R. J. YOUNG, *J. Mater. Sci.* **9** (1974) 2034.
35. D. M. SHINOZAKI and G. W. GROVES, *ibid.* **8** (1973) 1021.
36. I. L. HAY and A. KELLER, *J. Polym. Sci. C* **30** (1970) 289.
37. D. P. POPE and A. KELLER, *J. Polym. Sci.* **13** (1975) 533.
38. A. KELLER and D. P. POPE, *J. Mater. Sci.* **6** (1971) 453.
39. S. G. BURNAY, M. D. D. AERE and G. W. GROVES, *ibid.* **13** (1978) 639.
40. V. I. GERASIMOV, YA. V. GENIN and D. YA. TSVANKIN, *J. Polym. Sci., Polym. Phys. Edn* **12** (1974) 2035.
41. P. J. HENDRA, M. A. TAYLOR and H. A. WILLIS, *Polymer* **26** (1985) 1501.
42. N. S. J. A. GERRITS and Y. TERVOORT, *J. Mater. Sci.* **27** (1992) 1385.
43. Z. BARTCZAK, A. S. ARGON and R. E. COHEN, *Polymer* **35** (1994) 3427.
44. C. P. LAFRANCE, J. DEBIGARE and R. E. PRUDHOMME, *J. Polym. Sci., Polym. Phys. Edn* **31** (1993) 255.
45. J. A. H. M. MOONEN, W. A. C. ROOVERS, R. J. MEIER and B. J. KIP, *ibid.* **30** (1992) 361.
46. M. F. BUTLER, A. M. DONALD, W. BRAS, G. R. MANT, G. E. DERBYSHIRE and A. J. RYAN, *Macromolecules* **28** (1995) 6383.
47. M. E. VICKERS and H. FISCHER, *Polymer* **36** (1995) 2667.
48. J. W. H. KOLNAAR, A. KELLER, S. SEIFERT, C. ZSCHUNKE and H. G. ZACHMANN, *ibid.* **36** (1995) 3969.
49. V. GAUCHER-MIRI, P. FRANCOIS and R. SEGUELA, *J. Polym. Sci., Polym. Phys. Edn* **34** (1996) 1113.
50. D. HOFMANN, D. GEISS, A. JANKE, G. H. MICHLER and P. FIEDLER, *J. Appl. Polym. Sci.* **39** (1990) 1595.
51. W. WU, G. D. WIGNALL and L. MANDELKERN, *Polymer* **33** (1992) 4137.
52. S. J. SPELLS and E. U. OKOROAFOR, *ibid.* **35** (1994) 4590.
53. B. K. ANNS, J. STRIZAK, G. D. WIGNALL, R. G. ALAMO and L. MANDELKERN, *ibid.* **37** (1996) 137.
54. C. SCHIPP, M. J. HILL, P. J. BARHAM, V. M. CLOKE, J. S. HUGGINS and L. OIARZABAL, *ibid.* **37** (1996) 2291.
55. E. U. OKOROAFOR and S. J. SPELLS, *ibid.* **35** (1994) 4578.
56. D. I. BOWER, E. L. V. LEWIS and I. M. WARD, *ibid.* **36** (1995) 3473.
57. V. STRAUCH and M. SCHARA, *ibid.* **36** (1995) 3435.
58. J. C. RODRIGUEZ-CABELLO, M. ALONSO, J. C. MERINO and J. M. PASTOR, *J. Polym. Sci., Polym. Phys. Edn* **60** (1996) 1709.
59. N. ALBERLOA and J. PEREZ, *J. Mater. Sci.* **27** (1991) 2921.
60. A. N. GENT and S. MADAN, *J. Polym. Sci., Polym. Phys. Edn* **27** (1989) 1529.
61. C. S. CRUZ, F. J. B. CALLEJA, T. ASANO and I. M. WARD, *Phil. Mag.* **68** (1993) 209.
62. J. D. HALFMAN, *Polymer* **23** (1982) 656.
63. M. BEVIS and E. B. CRELLIN, *ibid.* **12** (1971) 666.
64. A. KELLEY and G. W. GROVES, "Crystallography of crystal defects" (Longman, London, 1970).
65. A. PETERLIN, *Polym. Engng Sci.* **18** (1978) 488.
66. D. C. PREVORSEK, H. B. CHIN and S. MURTHY, *Amer. Chem. Soc. Preprints, Polym. Mater. Sci. Engng* **70** (1993) 43.
67. E. W. FISHER and H. J. GODDAR, *J. Polym. Sci. C* **16** (1969) 4405.
68. R. S. PORTER, *Amer. Chem. Soc. Polym. Preprints*, **12** (1971) 39.
69. E. S. CLARK and L. S. SCOTT, *Polym. Engng Sci.* **14** (1974) 682.
70. J. CLEMENTS, R. JAKEWAYS and I. M. WARD, *Polymer* **19** (1978) 639.
71. T. -H. YU and G. L. WILKES, *ibid.* **37** (1996) 4675.
72. T. -H. YU and G. L. WILKES, *J. Rheol.* **40** (1996) 1079.
73. H. -Y. ZHOU and G. L. WILKES, *Polymer*. To appear.
74. J. A. ODELL, D. T. GRUBB and A. KELLER, *ibid.* **19** (1978) 617.
75. R. G. C. ARRIDGE and P. J. BARHAM, *J. Polym. Sci., Polym. Phys. Edn* **16** (1978) 1297.

76. D. GORITZ, Unpublished work.
77. C. J. CHOU, A. HILTNER and E. BEAR, *Polymer* **27** (1986) 369.
78. T. KAJIYAMA and M. TAKAYANAGI, *J. Macromol. Sci., Phys. B* **10** (1974) 131.
79. J. MARTINEZ-SALAZAR, J. V. GARCIA RAMOS and J. PETERMANN, *Intn. J. Polym. Mater.* **21** (1993) 111.
80. N. W. BROOKS, R. A. DUCKETT and I. M. WARD, *Polymer* **22** (1992) 1975.
81. N. W. BROOKS, A. P. UNWIN, R. A. DUCKETT and I. M. WARD, *J. Macromol. Sci.* **34** (1995) 29.
82. B. K. CARTER, PhD dissertation, Vol. I, Virginia Polytechnic Institute and State University, Blacksburg VA (1986).
83. H. O. KEITH, F. J. PADDEN and R. G. VADIMSKY, *J. Polym. Sci.* **4** (1966) 267.
84. J. R. BURNS, *J. Polym. Sci. A* **2** (1969) 593.

Received 26 February
and accepted 19 August 1997